Modulation of time-mean and turbulent flow by suspended sediment

Hadis Matinpour,[1,*] Sean Bennett,[2] Joseph Atkinson,[1] and Michele Guala[3]
[1]*Department of Civil, Structural and Environmental Engineering, University at Buffalo, Buffalo, New York 14228, USA*
[2]*Department of Geography, University at Buffalo, Buffalo, New York 14261, USA*
[3]*St. Anthony Falls Laboratory and Department of Civil, Environmental and Geo-Engineering, University of Minnesota, Minneapolis, Minnesota 55455, USA*

(Received 18 October 2018; published 25 July 2019)

Nearly all geophysical flows entrain, transport, and deposit sediment, and many studies have sought to define how the presence of suspended sediment can affect flow dynamics of the carrier fluid. Yet the mechanisms of turbulence modulation by suspended sediment remain poorly understood. Experiments were conducted in a mixing box to evaluate the effects of suspended sand on the turbulent flow generated by an oscillating grid placed near the bottom of the box. Two-phase particle image velocimetry was used to obtain velocity characteristics of the sediment and fluid phases separately. Boundary conditions included a clear-water flow and six sediment-laden flows for comparative purposes. A strong secondary circulation was observed within the mixing box due to the position of the grid and stroke length. As sediment loading increased, the depth affected by the secondary circulation, the mean and turbulent kinetic energy, and the total suspended-sediment concentration decreased while turbulent length scales increased. These features coincided with the formation of a stratified layer where high suspended-sediment concentration occurred. Key length scales related to the vertical extent of secondary circulation regions, vertical mixing, and maxima of suspended-sediment concentrations were defined and used to identify and explain the formation of this stratified layer and the modulation of flow. The results presented here demonstrate the marked effects that suspended sediment and the formation of a stratified layer have on turbulent flow dynamics within a mixing box, and these results are expected to have broader implications for the study and interpretation of a wide range of sediment-laden geophysical flows.

DOI: 10.1103/PhysRevFluids.4.074605

I. INTRODUCTION

Many gravity-driven, geophysical flows occurring on the Earth's surface are fully turbulent and they can very effectively entrain, transport, and deposit sediment. As such, these flows comprise at least two phases, the carrier fluid and the sediment in transport. It would seem logical that as the rate of sediment transport or volume concentration increases, either as bed load, suspended bed material, or wash load, the dynamic characteristics of the fluid would be measurably altered, as conditioned by sediment texture and particle-turbulence interactions. Wainwright *et al.* [1] suggested that the dynamics of the carrier fluids for all sediment-laden geophysical flows are significantly altered by the presence of the sediment in transport. Various disciplinary studies have sought to quantify the effects of sediment in transport on the carrier fluid in open channel flows [2], two-phase flow phenomena in engineering applications [3], and stratified flows in fluvial and marine environments [4], among others.

*hadismat@buffalo.edu

The presence of sediment in transport in rivers, and in particular suspended bed material, can potentially affect time-mean flow and turbulence in several ways. Vanoni and Nomicos [5] found experimentally that suspended sediment increased velocity gradients near the wall, and other studies have shown that suspended sediment altered additional time-mean parameters such as the von Kármán coefficient, the profile of downstream velocity, and bed friction in open channels [6–11]. Effects of suspended sediment on turbulence statistics have been reported by Best *et al.* [2], who showed that the addition of suspended sand over a plane bed increased turbulent intensities near the bed and decreased turbulence intensities in locations far from the bed. A similar effect was reported by Nezu and Azuma [12], who indicated negligible turbulent intensity modulation in locations far from a wall, while turbulent intensities increased in regions near the wall. Muste *et al.* [13] showed that turbulent intensities increased near the bed in comparison to clear-water conditions, but turbulent intensities were only slightly reduced away from the bed. Particle-turbulence interactions could also be related to particle size. Noguchi and Nezu [14] documented experimentally that particle size was a good criterion for turbulence modulation, and fluid-particle interaction was governed by the ratio of particle diameter to the Kolmogorov length scale. They indicated that when this ratio is less than 1 and particle diameter is less than the Kolmogorov length scale, then turbulence is suppressed. However, when particle diameter size is larger than the Kolmogorov length scale, then turbulence is enhanced in the presence of suspended particles. Revil-Baudard *et al.* [15] suggested that turbulent kinetic energy of the fluid increased in sediment-laden flows because of an increase in sweep and ejection events at the bed due to the moving sediment.

Within the context of two-phase flow dynamics, turbulence modulation of the carrier fluid has been related to specific particle-fluid phenomena and indices. Turbulence reduction in dilute suspensions has been attributed to three mechanisms: (1) enhanced inertia of particle-laden flows, (2) increased dissipation due to particle drag, and (3) enhanced viscosity [16]. Conversely, turbulent enhancement has been linked to two mechanisms: (1) enhanced velocity fluctuations due to wake dynamics and vortex shedding behind particles, and (2) buoyancy-induced motions due to density variations [16]. To characterize the relative impacts of these processes, criteria have been proposed to define conditions that enhance or reduce turbulence in the presence of suspended particles. Gore and Crowe [17] proposed that when the ratio of the particle diameter size to the fluid turbulence length scale is smaller than 0.1, fluid turbulence is suppressed, and fluid turbulence is enhanced when this ratio is greater than 0.1. Hestroni [18] proposed that the slip velocity between the particle and carrier fluid can be used to explain turbulent modulation. Elghobashi [19] asserted that the ratio of the particle response time to the fluid response time may be a good proxy for turbulent modulation. Picano *et al.* [20] investigated particle-laden turbulent flows with solid neutrally buoyant spheres at relatively high volume fractions, and showed that the mean velocities are markedly reduced in the presence of the solid phase and that the overall drag close to the bed increased with volume fraction.

Vertical stratification of the flow as a result of high suspended-sediment concentrations also has been reported in rivers and marine environments as a cause of flow modulation [21–24]. Noh and Fernando [25] reported that a stratified flow comprising a denser, sediment suspension layer overlain by a lighter, relatively sediment-free layer can form when the Richardson number R_i is greater than a specific magnitude of the Rouse number R_o (defined later). Ozdemir *et al.* [26] studied numerically the role of turbulence on fine particle transport in an oscillatory flow. They showed that as R_i increased, turbulence decreased due to the emergence and growth of a particle-induced stratified flow, consistent with the results of Noh and Fernando [25]. When R_i is larger than R_o, upward sediment flux is greater than the downward settling flux; sediments are maintained in suspension and produce a stratified flow. Wright and Parker [21] noted that higher concentrations of suspended sediment near a river bed produced a density gradient that created a buoyancy force, thus reducing turbulent eddy viscosity and sediment diffusivity. Cantero *et al.* [27] (see also Kneller *et al.* [28]) suggested that total turbulence suppression in dilute, noncohesive turbidity currents ($<1\%$ by volume) might be due to stratification. They showed that the product of R_i and R_o can be interpreted as the required energy to maintain sediments in suspension by turbulent flow, which can be used

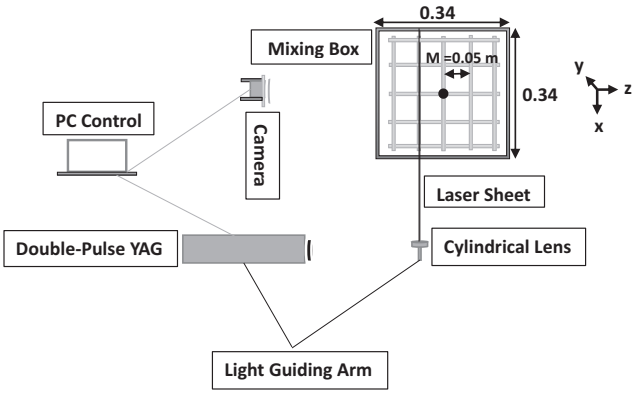

FIG. 1. Schematic top view diagram of the mixing box and PIV.

as an indicator of the turbulence modulation by suspended sand. Similar results were obtained by Hooshmand *et al.* [29], who conducted experiments to study turbulence structure in wave-supported mud layers. They noted that when the flow velocity was relatively high, a dense suspended-sediment stratified layer formed, which reduced turbulence.

Suspended sediment apparently can have different impacts on flow dynamics, but the specific physical mechanisms for such modulation are still not well known. The goal of the present research is to examine experimentally the effects of suspended sediment on the carrier fluid. To do this effectively, two important experimental conditions must be achieved. First, the experimental conditions must be reproducible, thus avoiding ambiguities related to varying boundary conditions. Second, the fluid phases and their time-mean and turbulent characteristics must be clearly discriminated from those of the sediment phase. To accomplish these goals, this study employed (1) a mixing box with an oscillating grid to generate reproducible turbulence and mixing, and (2) two-phase particle image velocimetry (PIV) at relatively high temporal and spatial resolutions. The objectives of the current paper are to document and describe the modulation of time-mean and turbulent flow by the presence of suspended sediment as a function of imposed sediment loading, and to identify and discuss the physical processes responsible for any measurable changes in the carrier fluid.

II. EXPERIMENTAL SETUP AND MEASUREMENT TECHNIQUES

Figure 1 shows a schematic diagram of the mixing box, which is nearly the same or identical to those used in many previous studies [30–33]. It is a rectangular polycarbonate tank of dimensions 0.32×0.32 m in cross section, 0.40 m high, and 0.01 m thick. An aluminum grid consisting of an intersecting mesh of 0.01-m-square rods and a mesh spacing of 0.05 m is located near the bottom of the box, which is attached to a stainless steel bar with an eccentric connection to an external electrical motor. The grid is located so that the lowest extent of its movement is always just above the bottom of the tank. For all tests reported here, the box is filled with tap water to a height of 0.27 m. Prior to each experiment, a desired amount of sand is distributed uniformly as a thin layer on the bottom of the box before the grid motion is initiated. The grid oscillation produces a series of jets and wakes that generate turbulence in the box, which is sufficient to suspend sand grains and maintain them in suspension.

Within a mixing box forced by an oscillating monoplanar grid, the magnitude of turbulence production P at the grid virtual origin is a function of the oscillating frequency f, stroke length S, and mesh size M [34,35]. In the present experiments, $f = 5$ Hz,$S = 0.05$ m, and $M = 0.05$ m; thus P is constant. Different volumetric concentrations of sand ϕ_v are used (0.3%, 0.45%, 0.6%, 0.9%, 1.2%, and 1.4%), the median grain diameter d_{50} of the sand is 0.37–0.4 mm, and particle density ρ_p is 2650 $\mathrm{kg/m^3}$.

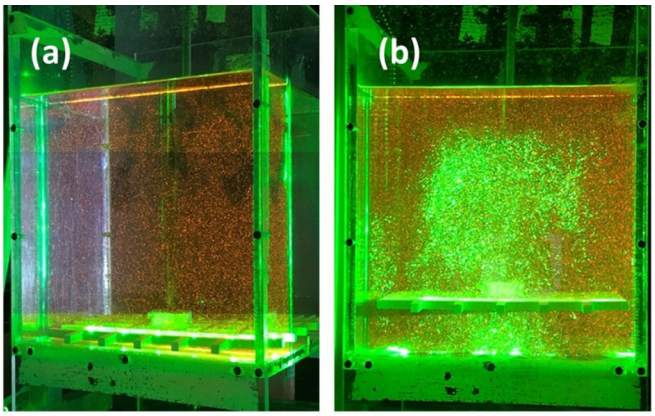

FIG. 2. Photographs of the mixing box illuminated by the laser sheet showing (a) tracer particles and (b) tracer particles and suspended sediment.

Particle image velocimetry (PIV) is used to measure velocities of the fluid and sediment phases. The PIV system consists of a high speed camera, a 50-mJ Nd-YAG dual-cavity laser emitting 532-nm light, and an external timing hub connected to a computer for data acquisition and synchronization (Fig. 1). A thin sheet 0.08 m from the sidewall in the x-y plane is illuminated by the laser light, where x is the horizontal distance measured from the left wall of the box and y is the vertical position measured upward from the highest position of the grid. Data are recorded from $x/B = 0.01$ to 0.99, where B is the box width, and extended vertically from $y/d = 0.02$ to 0.98, where d is the flow depth measured from the highest position of the grid to the water surface. For all tests reported here, $d = 0.22$ m.

To distinguish between the two phases, fluorescent Rhodamine B particles are employed as tracers for the fluid phase. These particles reflect laser light with a different color and wavelength (>570 nm, red in color) as compared to sand particles (Fig. 2). Once a test starts and reaches steady-state conditions, a long-pass optical filter is mounted on the camera lens to isolate only the reflectance of the fluorescent tracer particles. PIV analysis of these images provides the fluid phase velocities. A second series of images is then recorded after replacing the red filter with a green optical filter (530 nm) to record the reflectance from the sand particles only (the sediment turbulence data are not included here). To quantify the turbulence signals for each phase, 2400 paired images are captured in a 30-s period at 80 Hz. The time lapse between pulses is set to 2500 μs and interrogation areas applied in the cross-correlation algorithm are 32 × 32 pixels. The calibration image shows that each pixel corresponds to 0.14 mm and spatial resolution of the PIV data is calculated to be 4.4 × 4.4 mm. An adaptive cross-correlation algorithm within the commercial software (Dantec DYNAMIC STUDIO) is used to derive instantaneous velocities and vector maps based on the acquired paired images.

A MATLAB program is used to analyze the PIV images and calculate the suspended sand concentration distribution. Each sediment-laden image is divided into 32 × 32 pixel windows. Sand particles are identified for each window, and the number of particles is counted. As shown in Fig. 3, object size (in pixels) is plotted against light intensity for all identified objects for 400 sand images. The object intensity is defined as the average intensity of the pixel associated with the specific object. As shown in Fig. 4, some sand particles are completely illuminated in the laser sheet (particles 4 and 5), while other particles are partially illuminated (particles 1, 2, and 3). As the intensity narrows and sharpens, a smaller part of the sand particle is illuminated. All sand particles are counted in the identification code, independent of being totally or partially within the laser sheet. Objects with average intensities between 0.35 and 0.8 and sizes between 5 and 20 pixels are counted as sand particles (Fig. 3). Sand particles slightly in front of or behind the laser sheet produced weak

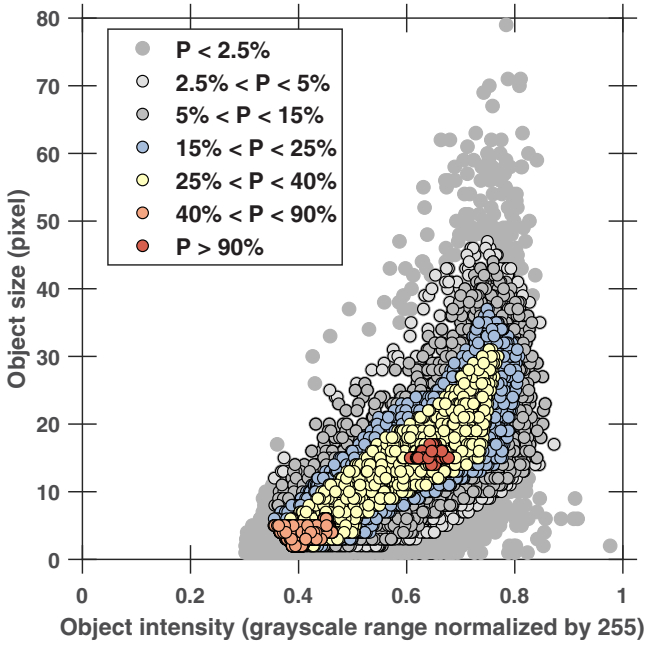

FIG. 3. Object size (in pixels) versus object intensity (gray-scale range normalized by 255) for all objects in 400 sand images recorded in 5 s; P is probability.

shadows; their signals are considered background noise and are subtracted from the image prior to analysis.

In all experiments, the thickness of the laser sheet is approximately 2.5 mm. Volumetric suspended sand concentration C based on the number of sand particles for each position in the planar image is defined using

$$C = \frac{n\frac{4}{3}\pi\left(\frac{d_{50}}{2}\right)^3}{V}, \tag{1}$$

where n is the number of sand particles in the window image (4.4 × 4.4 mm) and the volume V of the laser sheet at a given x-y is 48.4 mm^3.

All experiments were repeated several times for the same boundary conditions. Both the time-mean flow and turbulence results obtained from these repeated experiments are nearly identical.

III. RESULTS

A. Flow characteristics

Instantaneous and time-averaged flow statistics within the mixing box can be quantified using the PIV data for the tracer particles. Two-dimensional flow velocities are defined using the standard turbulence decomposition,

$$u' = u - [u], \tag{2}$$

$$v' = v - [v], \tag{3}$$

where u and v are the instantaneous horizontal and vertical velocity components, the brackets define time-averaged values at a point, and the primes indicate their fluctuating terms. The magnitude of

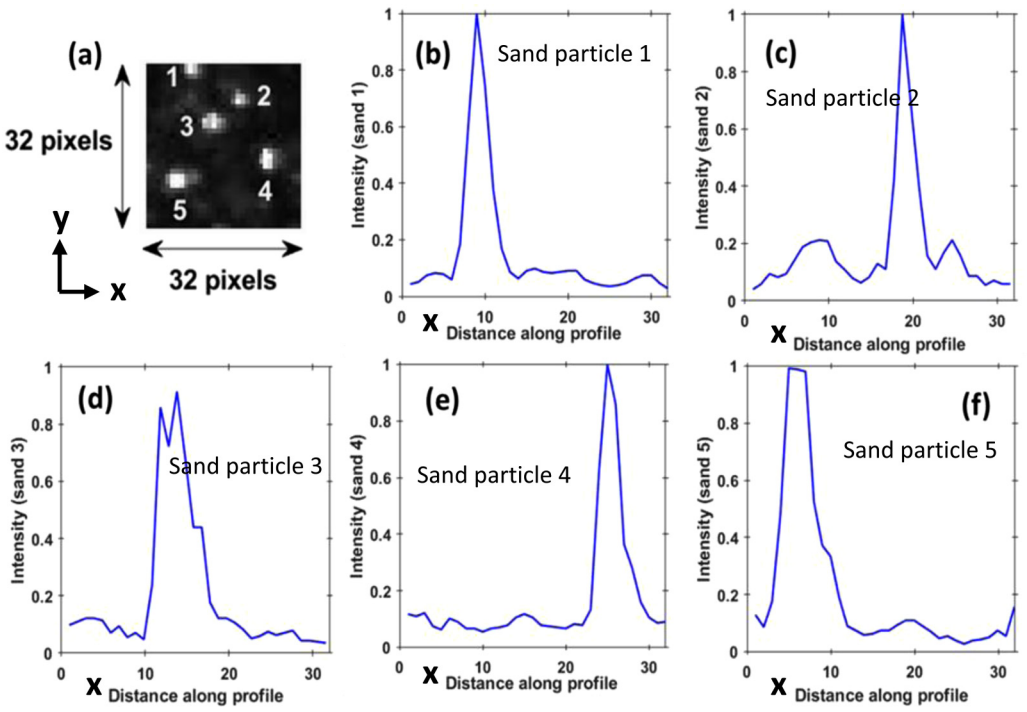

FIG. 4. For a sediment-laden PIV image, (a) 32 × 32 pixel window with five sand particles, and intensity profile versus horizontal distance along profile for sand particle (b) 1, (c) 2, (d) 3, (e) 4, and (f) 5.

the mean velocity V_f is defined by

$$V_f = ([u]^2 + [v]^2)^{0.5}. \tag{4}$$

Figure 5 shows the magnitude of the mean velocities in clear-water and sediment-laden conditions. Velocities in the clear-water experiment demarcate two symmetric circulation patterns in the flow field, extending to the top of the mixing box. This secondary circulation pattern has been observed in previous studies [32,33,36,37]. In most traditional mixing box experiments, secondary circulation flow is not a critical issue because the grid is located at the top or near the middle of the box, and smaller combinations of oscillation frequency and stroke length are employed [34,38,39]. For this study, a greater amount of kinetic energy at the bottom of the box was needed to suspended sediment and to maintain sediment in suspension, which necessitated the location of the grid near the bottom wall and a larger stroke length. With these conditions, a secondary circulation pattern of non-negligible intensity was produced.

The presence of sediment and the variation of sediment loading have a measurable effect on the secondary circulation within the box. The sediment in suspension has two effects on the secondary flow: (1) It decreases velocity magnitude, and (2) it decreases the depth affected by the secondary circulation cells. Both effects increase as sediment loading increases, which suggests an extension of the turbulence modulation mechanism from the fluctuating velocity field to the mean flow. A characteristic length scale can be defined as D_s, the height of the secondary circulation pattern within the box. This length scale is shown schematically in Fig. 5, and it is listed for all experiments in Table I. As sand loading increases, D_s decreases. It should be noted that total suspended sand concentration is not directly correlated to sand loading and observational results indicated that there is less sand in suspension as the total sand loading increases, which is discussed below.

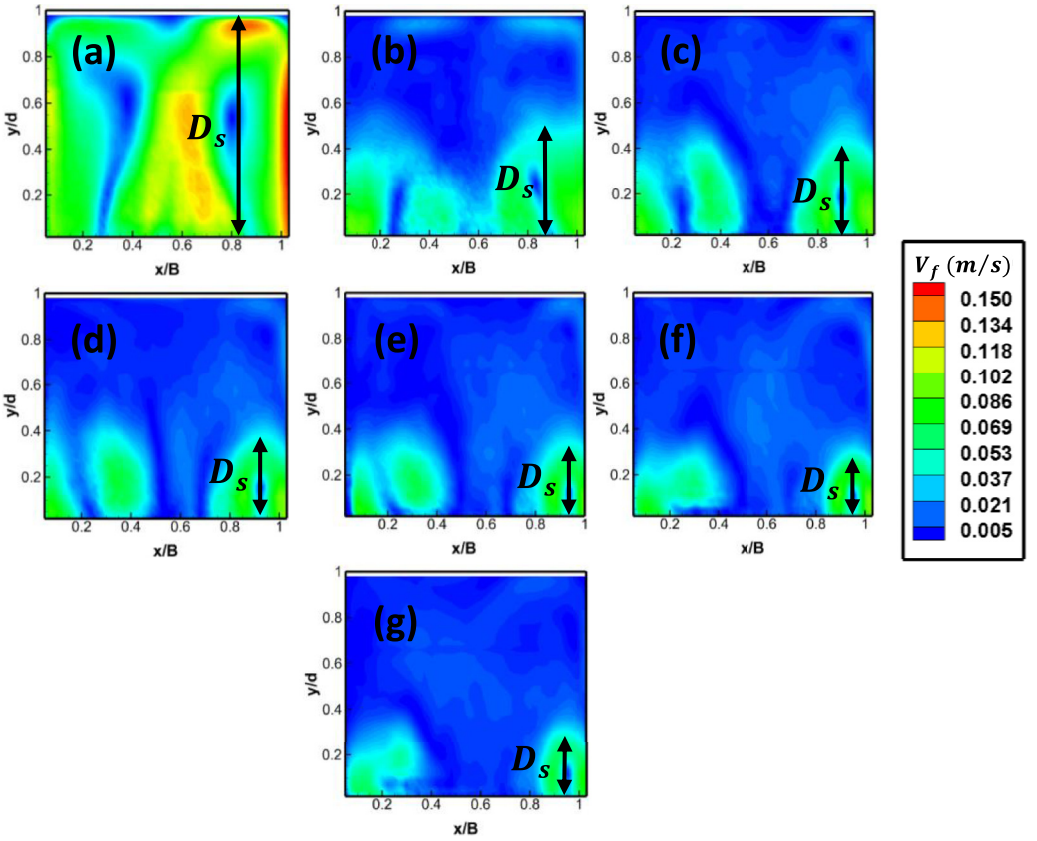

FIG. 5. Comparison of mean velocity magnitude (V_f) for (a) the clear water flow and for sand volume fractions of (b) 0.3%, (c) 0.45%, (d) 0.6%, (e) 0.9%, (f) 1.2%, and (g) 1.4%. D_s defines the height of the secondary circulation.

The mean kinetic energy of the fluid phase per unit mass MKE and its horizontally averaged value ⟨MKE⟩ are defined by

$$\mathrm{MKE} = 0.5([u]^2 + [v]^2), \tag{5a}$$

$$\langle \mathrm{MKE} \rangle = \frac{1}{B}\int_{x=0}^{B} \mathrm{MKE}\, dx. \tag{5b}$$

TABLE I. Summary of turbulence statistics, length scales, and suspended-sediment concentration for all experiments.

Volumetric sand concentration ϕ_v	T_{MKE} ($\mathrm{m}^2/\mathrm{s}^2$)	T_{TKE} ($\mathrm{m}^2/\mathrm{s}^2$)	T_{KE} ($\mathrm{m}^2/\mathrm{s}^2$)	D (m)	D_s (m)	D_c (m)	$T_{\langle C \rangle}$
0%	0.0190	0.010	0.030	NA	0.22	NA	NA
0.30%	0.0024	0.015	0.017	0.076	0.13	0.100	0.0044
0.45%	0.0021	0.011	0.013	0.071	0.11	0.033	0.0022
0.60%	0.0017	0.008	0.010	0.063	0.10	0.033	0.0020
0.90%	0.0015	0.007	0.008	0.052	0.09	0.029	0.0016
1.20%	0.0012	0.004	0.005	0.042	0.08	0.029	0.0014
1.40%	0.0008	0.003	0.003	0.038	0.07	0.029	0.0011

Horizontally averaged values of mean kinetic energy $\langle \mathrm{MKE} \rangle$ are plotted as a function of normalized height above the grid y/d in Fig. 6(a) for each experiment. In general, $\langle \mathrm{MKE} \rangle$ is greatest just above the grid, and it decreases toward the water surface. The clear-water values of $\langle \mathrm{MKE} \rangle$, however, are much larger than those observed in the sediment-laden flows. Moreover, as sand loading increases, $\langle \mathrm{MKE} \rangle$ decreases, and $\langle \mathrm{MKE} \rangle \to 0$ above the region of secondary circulation where $y > D_s$ (see Fig. 5).

The total mean kinetic energy of the fluid phase per unit mass T_{MKE} can be calculated using

$$T_{\mathrm{MKE}} = \frac{1}{d} \int_{y=0}^{d} \langle \mathrm{MKE} \rangle \, dy. \tag{6}$$

These values are listed in Table I. The value of T_{MKE} is relatively large for the clear-water flow, which is to be expected because of the clearly defined secondary circulation pattern shown in Fig. 5(a). The addition of suspended sediment, however, decreases T_{MKE} by more than an order of magnitude, even with relatively low sand loading. This decrease in T_{MKE} as the volumetric sand concentration ϕ_v increases is the result of suppressing the magnitude of the secondary circulation cell and the decrease in the length scale D_s (see Table I, Fig. 5). As ϕ_v increases from 0.3% to 1.4%, T_{MKE} decreases by two-thirds.

To quantify the effect of sand suspension on the turbulence, horizontal and vertical root-mean-square velocities of the fluid phase (u_{rms} and v_{rms}, respectively) and turbulent kinetic energy per unit mass TKE are defined as

$$u_{\mathrm{rms}} = [u'^2]^{0.5}, \quad v_{\mathrm{rms}} = [v'^2]^{0.5}, \tag{7}$$

$$\mathrm{TKE} = 0.5 \left(u_{\mathrm{rms}}^2 + v_{\mathrm{rms}}^2 \right). \tag{8}$$

Values of TKE can then be averaged horizontally using

$$\langle \mathrm{TKE} \rangle = \frac{1}{B} \int_{x=0}^{B} \mathrm{TKE} \, dx. \tag{9}$$

Values of $\langle \mathrm{TKE} \rangle$ for clear-water and sediment-laden conditions are shown in Fig. 6(b). For the clear-water condition, $\langle \mathrm{TKE} \rangle$ is a maximum near the grid and it decreases toward the water surface similar to previous studies [32–34]. The response of $\langle \mathrm{TKE} \rangle$ under sediment loading conditions, however, is more complicated. In general, as ϕ_v increases, $\langle \mathrm{TKE} \rangle$ decreases significantly. Yet when $\phi_v = 0.3\%$, $\langle \mathrm{TKE} \rangle$ increases for $y/d < 0.35$, but it decreases when $y/d > 0.35$ in comparison to the clear-water condition. When $\phi_v = 0.45\%$, there is no change in $\langle \mathrm{TKE} \rangle$ for $y/d < 0.25$, but $\langle \mathrm{TKE} \rangle$ decreases for $y/d > 0.25$ in comparison to the clear-water condition. As noted above, these experiments were repeated several times, especially using the clear-water conditions, and the results were nearly identical to those reported here.

The total turbulent kinetic energy of the fluid phase per unit mass T_{TKE} can be calculated using

$$T_{\mathrm{TKE}} = \frac{1}{d} \int_{y=0}^{d} \langle \mathrm{TKE} \rangle \, dy, \tag{10}$$

and these values are listed in Table I. With the addition of suspended sediment to the mixing box, or as ϕ_v varies from 0% to 1.4%, T_{TKE} decreases by approximately one order of magnitude.

Values of horizontally averaged total kinetic energy per unit mass $\langle T_{\mathrm{KE}} \rangle$ and the vertically integrated total kinetic energy per unit mass T_{KE} can be defined as

$$\langle T_{\mathrm{KE}} \rangle = \langle T_{\mathrm{MKE}} \rangle + \langle T_{\mathrm{TKE}} \rangle, \tag{11}$$

$$T_{\mathrm{KE}} = T_{\mathrm{MKE}} + T_{\mathrm{TKE}}. \tag{12}$$

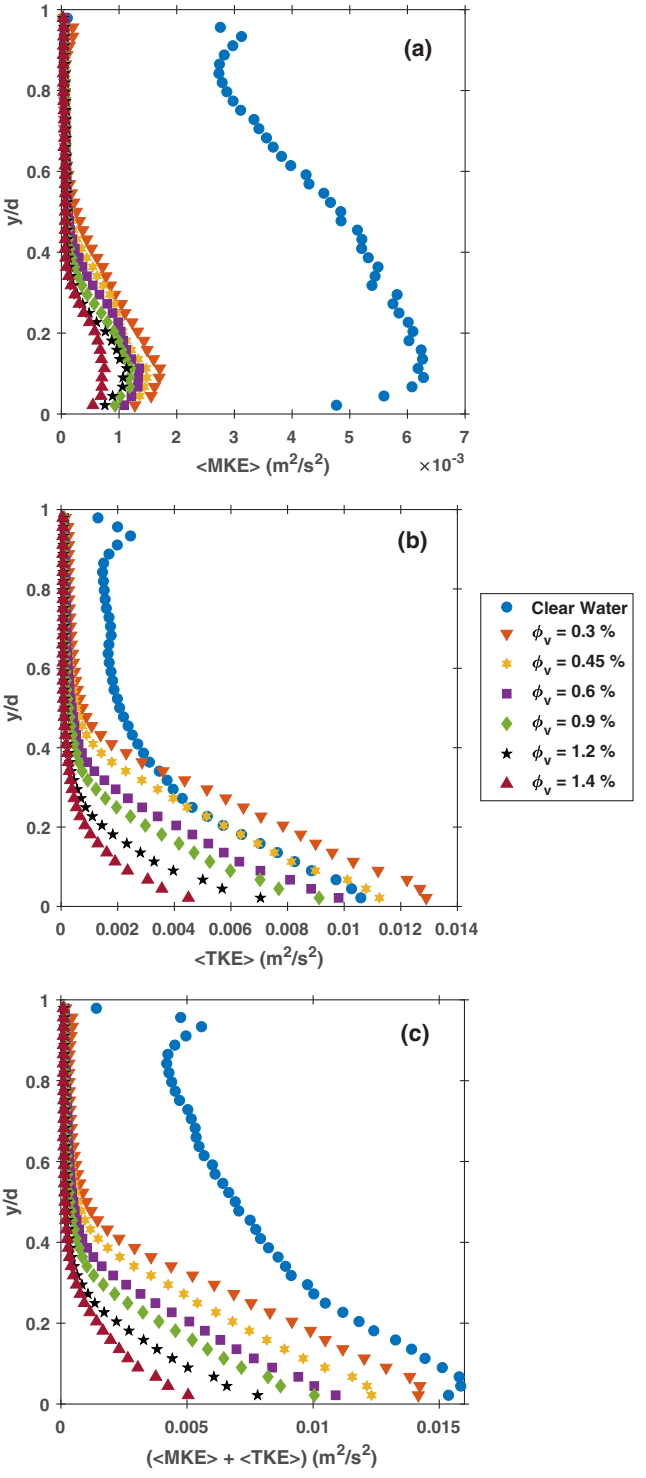

FIG. 6. Vertical profiles of horizontally averaged (a) mean kinetic energy, (b) turbulent kinetic energy, and (c) total kinetic energy.

Values of $\langle T_{\mathrm{KE}}\rangle$ are plotted as a function of y/d in Fig. 6(c), and values of T_{KE} are listed in Table I. In general, increases in ϕ_v markedly decrease $\langle T_{\mathrm{KE}}\rangle$ and T_{KE}, which decrease by an order of magnitude.

From Fig. 6, the decrease of $\langle \mathrm{MKE}\rangle$ due to the suppression of the recirculation cells [Fig. 6(a)] is also related to an altered energy transfer from the mean to the fluctuating velocity field, which may explain why $\langle \mathrm{TKE}\rangle$ increases close to the bottom for the smallest volume fraction [Fig. 6(b)]. The total kinetic energy of the flow exhibits a robust decreasing trend with increasing volume fraction [Fig. 6(c)] that suggests an overall flow suppression induced by the suspended sediments consistent with stratified flows.

To further explore the effect of suspended sediment on turbulence, the degree of anisotropy is considered. Previous studies have assumed that oscillating-grid turbulence in clear water is mainly isotropic [34,35,40]. Here, horizontally averaged values of turbulent kinetic energy per unit mass $\langle \mathrm{TKE}\rangle$ can be normalized by horizontally averaged values of $\langle v_{\mathrm{rms}}\rangle^2$ to define a nondimensional turbulent kinetic energy TKE*,

$$\mathrm{TKE}^* = \frac{\langle \mathrm{TKE}\rangle}{(\langle v_{\mathrm{rms}}\rangle)^2} = \frac{1}{2}\left[\left(\frac{\langle u_{\mathrm{rms}}\rangle}{\langle v_{\mathrm{rms}}\rangle}\right)^2 + 1\right]. \tag{13}$$

For isotropic turbulence, values of $\mathrm{TKE}^* \approx 1$. As shown in Fig. 7(a), values of TKE* in clear-water conditions appear to be invariant with flow depth, maintaining values close to 0.8. This result indicates that $\langle u_{\mathrm{rms}}\rangle$ is slightly less than $\langle v_{\mathrm{rms}}\rangle$, and this relationship is independent of height above the bed. In the sediment-laden conditions, the distributions of TKE* are divided into three distinct regions [shown schematically in Fig. 7(b)]. Near the grid, values of TKE* range from about 1.1 to 1.5 as sediment loading increases, and turbulence within this region can be characterized as anisotropic where $\langle v_{\mathrm{rms}}\rangle < \langle u_{\mathrm{rms}}\rangle$. Closer to the water surface, TKE* values range from about 0.9 to 1.0, which is indicative of isotropic turbulence. These two layers are separated in space by a zone of transition. The thickness of the lower layer, or the vertical distance from the grid to the transition area, defines a second characteristic length scale D [Fig. 7(b)]. Values of D listed in Table I show that as sand volume fraction increases, D decreases and thus turbulence anisotropy increases in regions near the grid. Profiles of TKE* in the sediment-laden flows also show abrupt changes, which depict vertical confinement of turbulence mixing within the layer defined by D.

The importance of the length scale D in the sediment-laden flows, which defines the length of confinement of vertical mixing, can be demonstrated as follows. When values of $\langle \mathrm{TKE}\rangle$, $\langle v_{\mathrm{rms}}\rangle$, and $\langle u_{\mathrm{rms}}\rangle$ at $y = D$ (denoted by the subscript D) are used to normalize turbulence parameters, all the normalized values collapse onto single curves when plotted as functions of normalized height y/D (Fig. 8). This systematic behavior across all volumetric suspended-sediment concentrations strongly suggests that the vertical variations of turbulence within the mixing box could be explained, in whole or in part, by the existence of a layer of confined vertical mixing.

B. Turbulent length scales

Integral length scales are calculated to further evaluate the effect of suspended sand on turbulence characteristics and directional dependencies. Horizontal ζ_x and vertical ζ_y integral length scales are calculated using a two-point correlation approach [41]:

$$R_{xx}(\chi, x, y) = [u'(x, y, t)u'(x + \chi, y, t)], \quad R_{yy}(\chi, x, y) = [v'(x, y, t)v'(x, y + \chi, t)], \tag{14}$$

$$\zeta_x(x, y) = \frac{1}{R_{xx}(0, x, y)}\int_0^{\chi_0} R_{xx}(\chi, x, y)d\chi, \quad \zeta_y(x, y) = \frac{1}{R_{yy}(0, x, y)}\int_0^{\chi_0} R_{yy}(\chi, x, y)d\chi, \tag{15}$$

where χ is the spatial lag and χ_0 is the spatial lag where the correlation function first becomes zero. These values also can be horizontally averaged, similar to velocity values as above (Fig. 9). For the clear-water condition, spatially averaged horizontal $\langle \zeta_x\rangle$ and vertical $\langle \zeta_y\rangle$ integral length scales increase from the grid, from about 0.015 to 0.020 m near the grid to a maximum of about

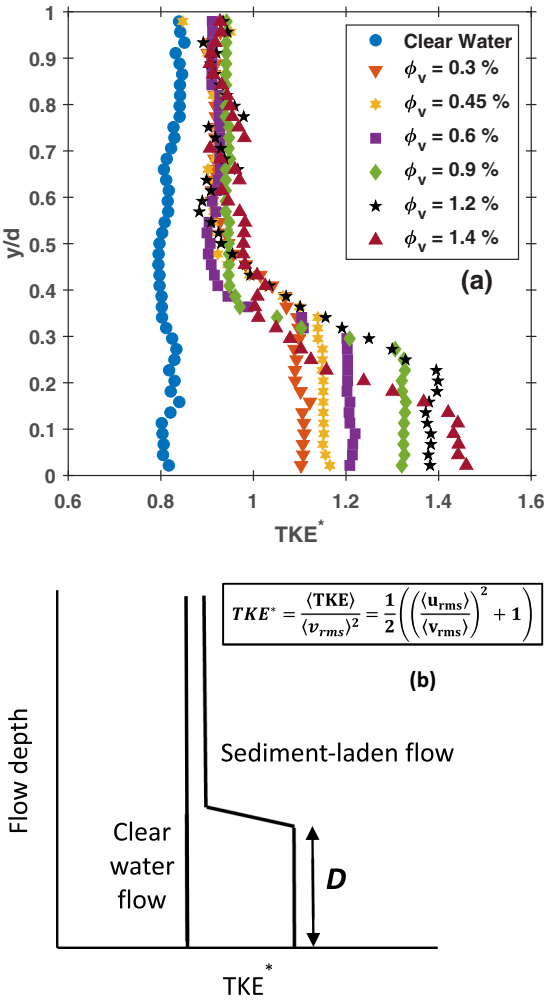

FIG. 7. Vertical profiles of (a) actual and (b) schematic ⟨TKE⟩ normalized by horizontally-averaged $\langle v_{\rm rms}\rangle^2$.

0.04–0.05 m near the water surface. These length scales are close in magnitude to the stroke S and mesh size M, or about 0.05 m. The value of $\langle\zeta_x\rangle/\langle\zeta_y\rangle$ is a measure of the distortion of the turbulent eddies generated by the oscillating grid. For the clear-water condition, $\langle\zeta_x\rangle/\langle\zeta_y\rangle = 0.85$ to 1.0 throughout the flow depth [Fig. 10(a)], suggesting that the eddies are nearly circular in shape, consistent with previous studies [30,36,39].

The presence of suspended sediment has a marked effect on turbulent length scales. In sediment-laden conditions, $\langle\zeta_x\rangle$ increases significantly in comparison to the clear-water condition at comparable distances from the grid. As sediment loading increases, the minimum values of $\langle\zeta_x\rangle$ increase from about 0.02 to 0.04 m near the grid, whereas their maximum values increase from about 0.06 to 0.15 m at locations away from the grid. Changes in $\langle\zeta_y\rangle$ increase from about 0.02 to 0.04 m near the grid, whereas their maximum values increase from about 0.06 to 0.11 m at distances away from the grid. These maxima of $\langle\zeta_x\rangle$ and $\langle\zeta_y\rangle$ near the water surface also increase with sediment loading. For both $\langle\zeta_x\rangle$ and $\langle\zeta_y\rangle$ in sediment-laden conditions, all length scales are larger than those observed in the clear-water conditions, and the maxima are much larger than the S and M length scales.

The shape of the turbulent eddies changes when suspended sediment is present. Figure 10(a) shows the length scale ratio $\langle\zeta_x\rangle/\langle\zeta_y\rangle$ as a function of height above the grid. Near the grid where

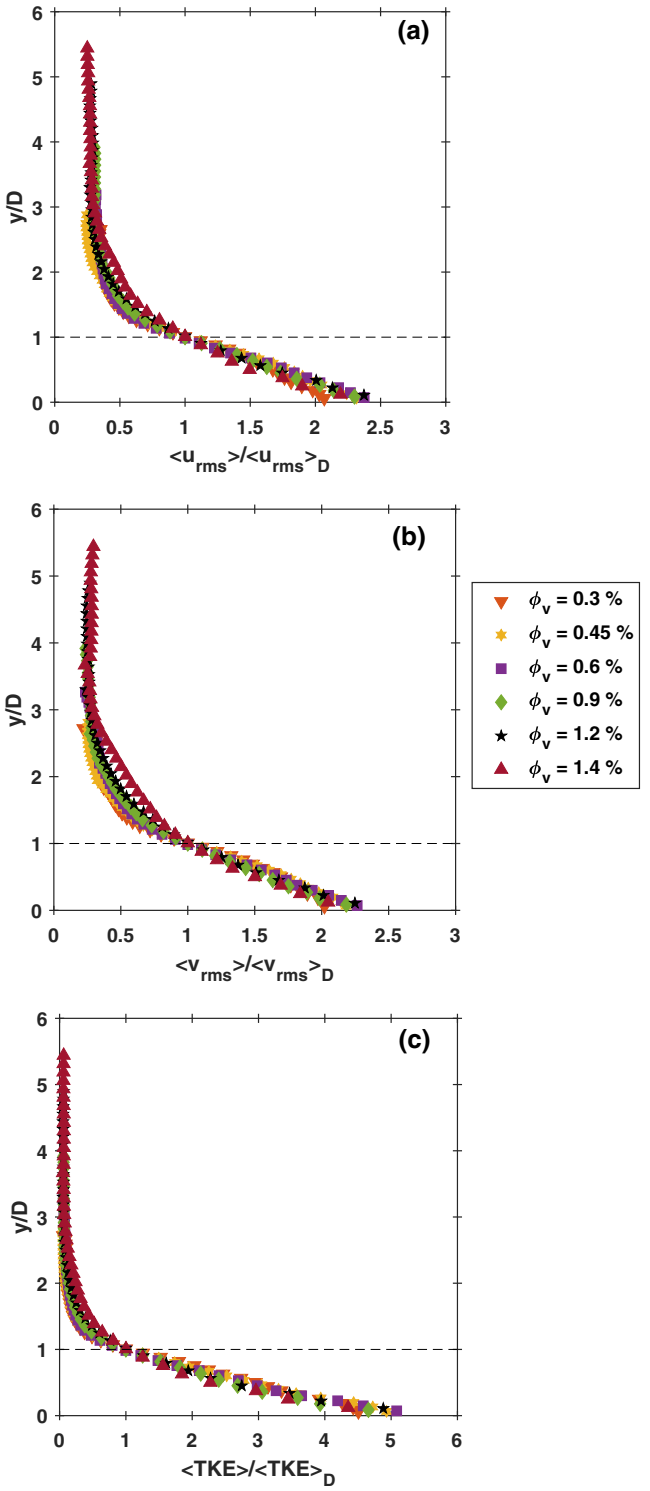

FIG. 8. Vertical profiles of horizontally averaged (a) u_{rms}, (b) v_{rms}, and (c) TKE all normalized by the value at the interface depth D.

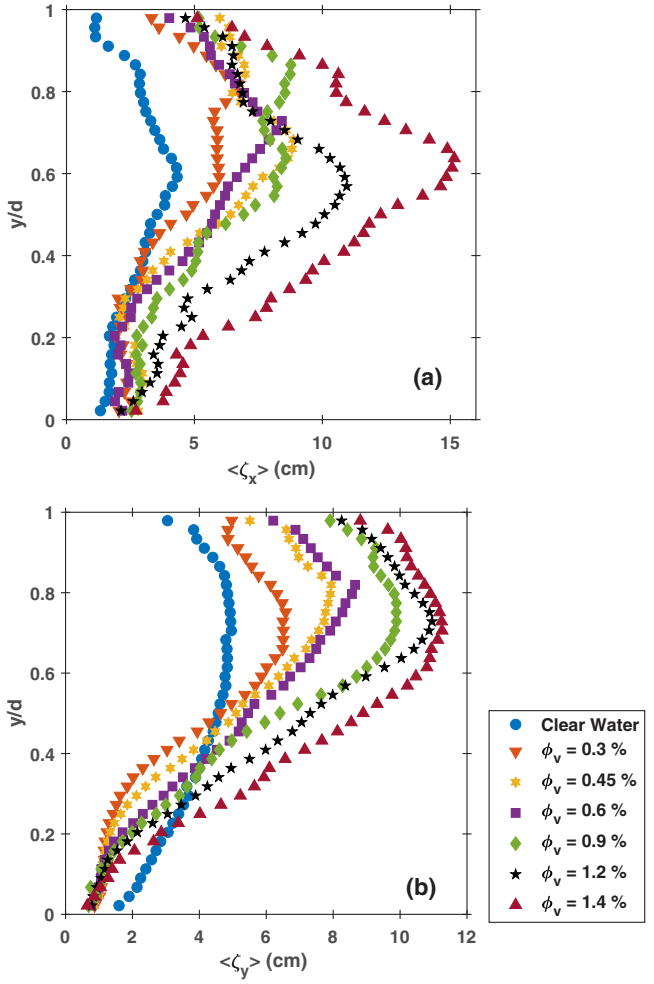

FIG. 9. Vertical profiles of horizontally averaged (a) horizontal and (b) vertical integral length scale.

$y/d < 0.3$, $\langle \zeta_x \rangle / \langle \zeta_y \rangle = 1.5$ to 4.0 and increases toward the grid. At larger distances from the grid when $y/d > 0.3$, $\langle \zeta_x \rangle / \langle \zeta_y \rangle = 1.0$ to 1.5. This suggests that eddies close to the bottom wall, identified as spatially correlated flow regions, have a larger horizontal axis compared to their vertical axis. They become more spherical toward the water surface where sediment concentration is much more diluted, while $\langle \zeta_x \rangle / \langle \zeta_y \rangle$ always remains large when suspended-sediment concentration is high. Variations in eddy size in sediment-laden conditions can be related to the confined vertical mixing zone near the grid. Figure 7 defines the length scale D, which is the length of confinement of vertical mixing. The values of $\langle \zeta_x \rangle / \langle \zeta_y \rangle$ are plotted as a function of y/D in Fig. 10(b). This normalization clearly demarcates a region of flattened eddies where $y/D < 1$ and $\langle \zeta_x \rangle / \langle \zeta_y \rangle \gg 1$, and a region of more circular eddies where $y/D > 1$ and $\langle \zeta_x \rangle / \langle \zeta_y \rangle = 1.0$ to 1.5. Thus the observed changes in the integral length scales can be related to near-grid vertical mixing processes, and to some extent, to the highly concentrated sediment layer.

C. Suspended sand concentration profiles

Discrimination of the sediment phase within the mixing box can be used to quantify the distributions of suspended sediment. Horizontally averaged suspended-sediment concentration $\langle C \rangle$

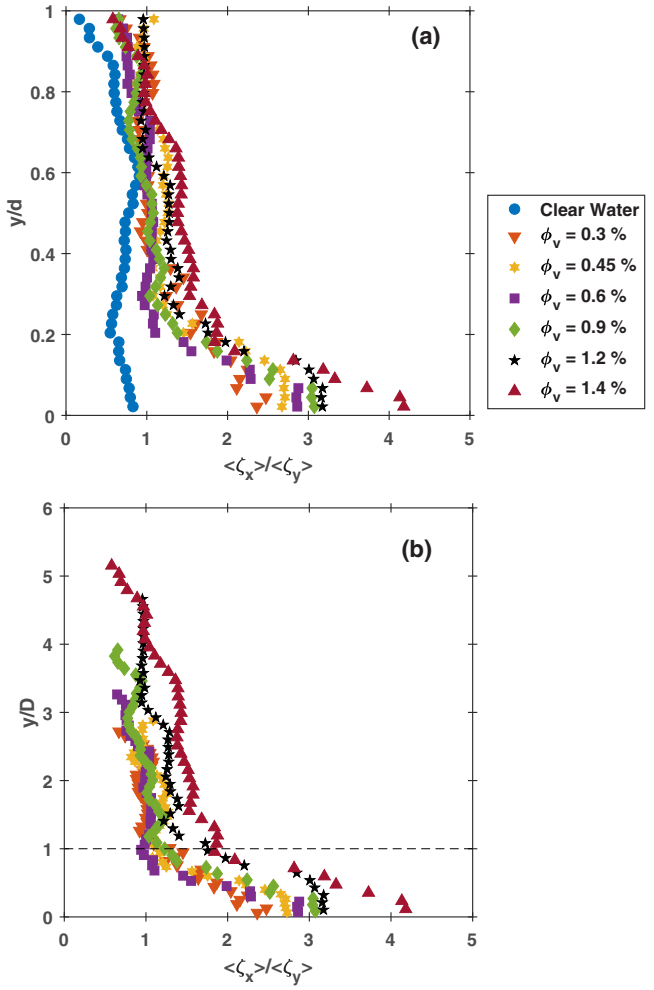

FIG. 10. Vertical profiles of the horizontal integral length scale to the vertical integral length scale as a function of (a) y/d and (b) y/D.

is defined as

$$\langle C \rangle = \frac{1}{B} \int_{x=0}^{B} C dx. \tag{16}$$

Figure 11(a) displays vertical profiles of $\langle C \rangle$ for all experiments. In general, $\langle C \rangle$ reaches a maximum value just above the grid and decreases rapidly toward the water surface. Although the amount of sand placed into the box increases, the volumetric suspended-sediment concentration within the flow decreases. The total volumetric suspended-sediment concentration for each experiment $T_{\langle C \rangle}$, defined by the laser sheet, can be calculated using

$$T_{\langle C \rangle} = \frac{1}{d} \int_{y=0}^{d} \langle C \rangle dy, \tag{17}$$

and these values are listed in Table I. While $T_{\langle C \rangle}$ shows a strong inverse relationship with ϕ_v, the observed variations in $T_{\langle C \rangle}$ are positively correlated with values of T_{KE}.

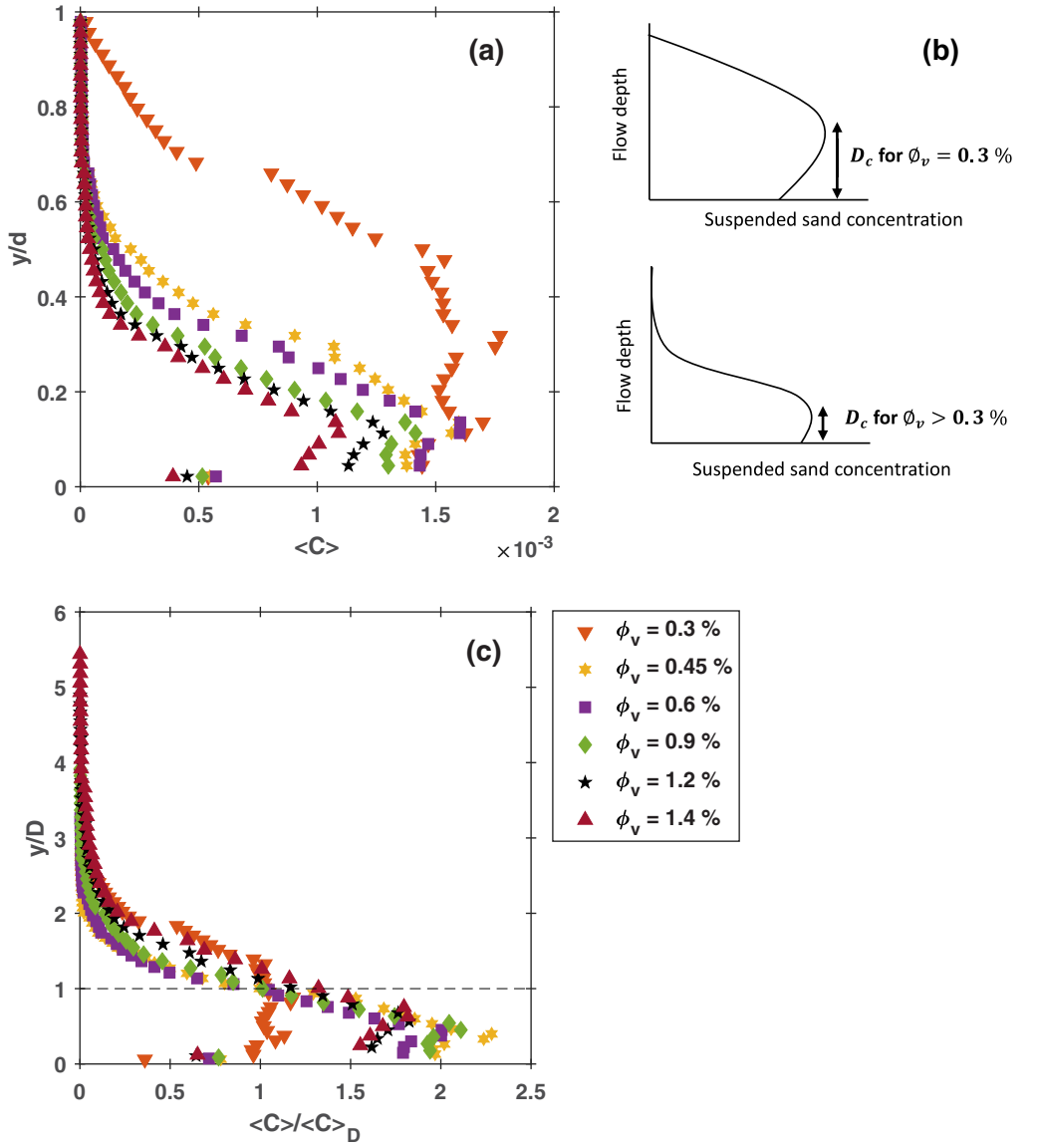

FIG. 11. Vertical profiles of horizontally averaged volumetric suspended sand concentration versus y/d as (a) measured and as a (b) schematic, and (c) suspended sand concentration values normalized by suspended sand concentration value at interface depth D.

Vertical distribution of suspended-sediment concentration can be used to define a third characteristic length scale. The parameter D_c is defined as the distance above the grid where suspended-sediment concentration attains a maximum value. These length scales for all sediment-laden experiments are listed in Table I, which shows that $D_c = 0.10$ m for $\phi_v = 0.30\%$, but $D_c \approx 0.03$ m when $\phi_v \geqslant 0.45\%$. Returning to Fig. 11, $\langle C \rangle$ can now be scaled by the concentration observed at D, or $\langle C \rangle_D = \langle C \rangle|_{y=D}$, and the height above the grid can be scaled by D as noted earlier. By adopting these normalizing parameters, $\langle C \rangle / \langle C \rangle_D$ first increases then decreases when $y/D \leqslant 1$, whereas $\langle C \rangle / \langle C \rangle_D$ assumes a distribution of suspended sediment similar to a Rouse profile when $y/D > 1$.

TABLE II. Summary of characteristic scale variables and important nondimensional numbers based on Noh and Fernando's definitions [25] (see text for definitions).

Volumetric sand concentration ϕ_v	L (m)	V (m/s)	W	R_o	R_i	$2.2(R_o)^2$
0.30%	0.010	0.110	0.23	0.45	3.02	0.45
0.45%	0.010	0.100	0.36	0.50	5.89	0.55
0.60%	0.009	0.090	0.33	0.56	6.00	0.68
0.90%	0.009	0.088	0.33	0.57	6.16	0.71
1.20%	0.008	0.075	0.26	0.67	6.18	0.98
1.40%	0.008	0.060	0.22	0.83	8.14	1.53

IV. DISCUSSION

The experimental results presented herein provide compelling empirical evidence that the presence of suspended sediment markedly affects the time-mean and turbulent flow generated by an oscillating grid in a mixing box. Noh and Fernando [25] suggested that two important nondimensional numbers controlling dispersion of suspended particles by grid-oscillation turbulence are the Rouse number R_o and Richardson number R_i, defined as

$$R_o = \frac{w_s}{V}, \tag{18}$$

$$R_i = \frac{g^* LW}{V^2}, \tag{19}$$

where $g^* = g(\rho_p - \rho_f)/\rho_f$ is reduced gravity affecting the sand particles; g is gravitational acceleration; ρ_f is fluid density; w_s is particle settling velocity; and L, V, and W are the characteristic length, velocity, and concentration scales, respectively. They asserted that if R_o is large enough, suspended particles settle rapidly and the suspended particle concentration profile monotonically decreases to zero with increasing height above the grid. When $R_i > 2.2(R_o)^2$, they found that upward buoyancy forces exceed downward settling forces and suspended particle concentration tends to be uniform within the near-grid region and a stratified layer or a front forms. Michallet and Mory [42] also demonstrated mathematically that the behavior of fine-grained sediments in suspension by purely diffusive turbulence, as ideally generated in oscillating-grid tanks, depends on R_o and the product of R_o and R_i. They showed that for small R_o, a concentrated suspension (stratified) layer is observed with a homogenous particle concentration, and its depth is a function of $R_o\, R_i$.

In this study, R_o and R_i are determined and characteristic scale variables are defined based on Noh and Fernando [25]. These include $g^* = 16.12\,\mathrm{m/s^2}$, $w_S = 0.05\,\mathrm{m/s}$ for sand with d_{50} between 0.37 and 0.40 mm ([43]; assuming no effects from turbulence, see, e.g., [44]), $L = l = \zeta_y|_{y=0}$, $V = \mathrm{TKE}^{0.5}|_{y=0}$, and $W = \frac{1}{D_c}\int_{y=0}^{D_c} \langle C\rangle dy$, which is average suspended-sediment concentration in depth D_c. These characteristic scales and the values of R_o and R_i for different boundary conditions are listed in Table II. In all experiments, R_i is larger than R_o, and as sand loading increases, both R_o and R_i increase. Using these values, Noh and Fernando's [25] criterion suggests that in all experiments reported here, a front or stratified layer should form (see Table II), which is shown herein. Suspended-sediment concentration profiles consist of two parts, a relatively uniform high-concentration layer near the grid, and a decreasing concentration distribution with height above it. In fact, the distribution of suspended-sediment concentration in the current experiment also satisfies the criteria for the formation of a front (see Fig. 11).

Yet the results need to be examined carefully, since many changes are occurring in tandem. To facilitate the discussion and interpretation of these results, a conceptual diagram is constructed to capture the observed particle-fluid interactions (Fig. 12). In clear-water conditions, the oscillating

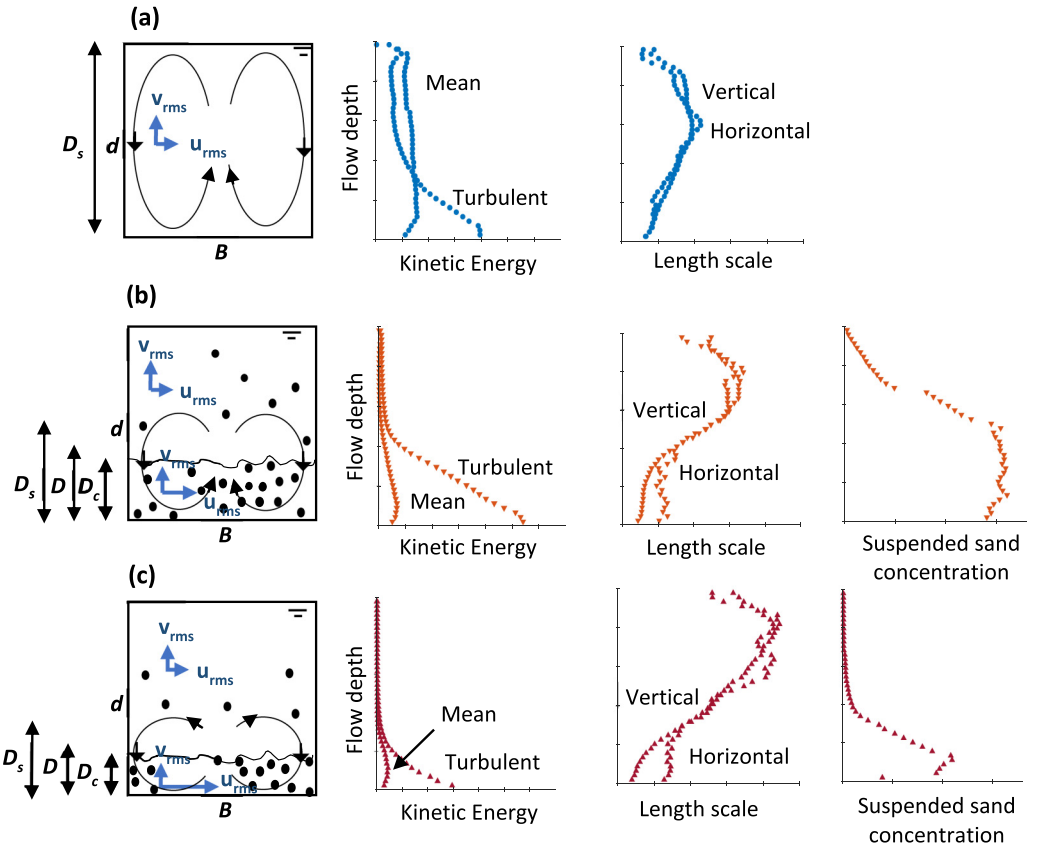

FIG. 12. Conceptual model for interaction between flow dynamics and suspended sand, for (a) clear-water flow, and sediment-laden flow at (b) low and (c) high loading.

grid produces turbulence near the bottom of the mixing box [Fig. 12(a)]. Turbulent kinetic energy has a maximum value near the grid, and it decreases toward the water surface. Integral turbulent length scales increase toward the water surface, and these relatively circular eddies scale in size with the grid stroke length and mesh size. Secondary circulation cells with an associated mean kinetic energy are created and scale with flow depth, presumably as a direct result of the grid being placed close to the bottom of the box and the relatively large stroke length employed.

Once sediment is placed into the box and suspended, flow is measurably altered. The magnitude of the mean kinetic energy and the spatial scale of the secondary flow cells decrease in response to the presence of suspended sediment even at relatively low concentration [Fig. 12(b)]. While total kinetic energy decreases in comparison to the clear-water conditions, the total turbulent kinetic energy increases near the bottom due to the presence of suspended sediment and the conversion of mean kinetic energy into turbulent kinetic energy [see Fig. 6(b)]. The vertical distribution of turbulent kinetic energy also changes. Values of $\langle \mathrm{TKE} \rangle$ increase near the grid and decrease at distances far from the grid, and a confined region of turbulent mixing can be clearly identified, as denoted by D. This near-grid layer contains relatively high and nearly invariant concentrations of suspended sediment. Integral length scales also change; turbulence length scales increase in size with sediment loading, but they become relatively flatter (more elliptical) in near-grid regions.

Increased sediment loading in the box further modulates the turbulent flow field. As sediment loading increases, the mean and turbulent kinetic energy decrease markedly, the magnitude and spatial extent of the secondary circulation cells diminish, and the region of confined vertical mixing

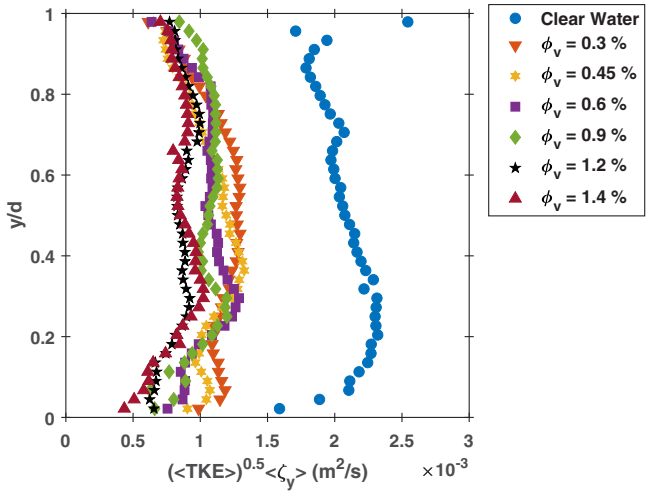

FIG. 13. Vertical profiles of fluid eddy viscosity for all experiments.

is reduced [Fig. 12(c)]. The total concentration of suspended sediment decreases as sediment loading increases, clearly the result of reduced ⟨TKE⟩ values. Length scales for the turbulent eddies increase with sediment loading, becoming much larger in scale in comparison to the grid stroke length and mesh size, especially as the distance from the grid increases. Note that a linear increase in the eddy size with distance from the grid is a common feature of oscillating-grid turbulence [34,35,38]. The modulation of eddy characteristics due to sediment loading denotes a marked change in the structure of turbulence.

It is clear that the presence of suspended sediment decreases the mean and turbulent kinetic energy in the mixing box. This is consistent with the results reported by Bennett *et al.* [32,33]. Yet as soon as sediment is added to and suspended in the flow, kinetic energy decreases and stratification occurs, as denoted by the length scales D and D_c. Huppert *et al.* [30] observed the formation of a stable self-limited layer of suspended sediment in their mixing box experiment, separated from the overlying layer by a sharp density interface, provided that a certain minimum mass of sediment is held in suspension. This observation suggests a reduction in kinetic energy due to the presence of suspended sediment.

The occurrence of a density interface affects the magnitude and length scales of turbulence. The experimental results of Hannoun *et al.* [45] showed that close to a density interface, TKE and turbulence anisotropy increased and turbulent eddies were flattened. The numerical results of Ozdemir *et al.* [26] showed that a suspended-sediment-induced stable density interface formed near the bed in an oscillatory flow and that turbulence was attenuated near the water surface. These results are consistent with the findings presented herein.

Flow stratification within the mixing box decreases turbulent kinetic energy and increases turbulent length scales with increased sediment loading, but the combined effect decreases fluid eddy viscosity. Noh and Fernando [25] defined fluid eddy viscosity K^* in a mixing box as

$$K^* = c_\mu \mathrm{TKE}^{0.5} l, \tag{20}$$

where c_μ is a constant and l is the length scale of turbulence. Using $\zeta_y = l$ for each height above the grid, Fig. 13 shows the variation of $\langle \mathrm{TKE} \rangle^{0.5} \zeta_y$ as a function of y/d. For clear-water conditions, eddy viscosity is uniform with depth because TKE values decay away from the grid by a power law with exponent $-2(\mathrm{TKE} \propto y^{-2})$ and integral length scale increases linearly with depth ($l \propto y$) [34,35,39,46]. Assuming c_μ is constant, the values of K^* for sediment-laden flows are distinctively smaller than the clear-water condition (50% or more smaller), and K^* decreases with sediment

loading (reduced by as much as 75% for $\phi_v = 1.4\%$). Flow stratification due to suspended sediment and a decrease in fluid eddy viscosity (or near-bed turbulence) has been observed in sediment-laden rivers [21], coastal and estuarine environments [29,47], and turbidity currents in the ocean [27]. The data presented herein are consistent with these previous results.

Turbulence suppression in the mixing box is due to the creation of a stratified layer as a direct result of the suspension of sediment. As noted, a stratified layer with confined vertical mixing forms in response to sediment in suspension. As sediment loading increases for the given oscillation frequency, T_{KE}, $T_{\langle C\rangle}$, D, and K^* all decrease and ζ_x and ζ_y increase. Any decrease in T_{TKE} and K^* would reduce the upward sediment flux [30] and the amount of sediment maintained in suspension [48].

Three characteristic length scales are recognized within the mixing box. These length scales denote the extent of the secondary circulation D_s, the height of the confined vertical mixing D, and the height of maximum suspended-sediment concentration D_c. Within the steady-state stratified layer, it can be assumed that the settling rate of particles within the mean flow is equal to the vertical transport of sediment by diffusion using the settling-diffusion equation, or $\langle C\rangle([v] - w_s) = K^* \frac{dC}{dy}$. In the current experiment, $\langle C\rangle([v] - w_s) \ll [v]$ (see Fig. 5), so the vertical transport rate of particles (or their turbulent diffusion upwards) is much smaller than the vertical velocity of the secondary circulation cell. This would suggest that D_c and D, which are closely related, are less than D_s. On the basis of the empirical observations herein, $D_s > D > D_c$, and these values are strongly correlated to variations in T_{KE} and T_{TKE} (Table I).

In the classic studies employing mixing boxes, the theoretical relationships to predict the distributions and magnitudes of turbulence with distance from the grid do not include the lengths D_s, D, and D_c for the simple reason that they did not exist or they were unrecognized [34,35]. In the current experiment, however, these length scales are pertinent because (1) the grid is positioned near the bottom of the box, which generates a secondary flow, and (2) a stratified layer composed of suspended sediment is created near the grid, which affects vertical profiles of turbulent kinetic energy and concentration profiles. These characteristic length scales then can be used to normalize distance from the grid as well as to define important turbulence and concentration parameters. In doing so, the normalized experimental data display self-similarity; data from all sediment-laden experiments collapse reasonably well onto single curves (see Figs. 8, 10, and 11). It is inferred here that such vertical variations in turbulence and sediment concentration within the sediment-laden flows are strongly conditioned, if not controlled, by the thickness D of the stratified layer and its fluid dynamic characteristics.

As sediment loading increases, the amount of sediment observed at the bottom of the box increases. This sediment created discrete piles between the mesh bars. It is possible that the presence of this sediment below and within the grid could further modulate turbulent flow and stratification effects above the grid. Using a mixing box, Huppert *et al.* [30] noted that as sediment loading increased, the depth of the sediment present on the bottom of the box increased. They too suggested this sediment could alter the bottom boundary conditions and affect the grid-generated turbulence in this region.

It should be noted that all data collected are within a single plane (at 0.08 m from the sidewall, or at 25% of the box total width). The time-averaged and turbulent flow fields likely exhibit spatial variations as a function of the distance from the box side wall [49]. These variations could alter the resultant magnitudes of secondary circulation and turbulent kinetic energy as the flow responds to the imposed suspended-sediment load, but the qualitative effects of suspended sediment on turbulence observed here are not expected to change.

Lastly, it is worth noting that some turbulent modulation criteria (e.g., [17–19]) are based on particle diameter size. These criteria suggest that grain diameter size (relative to the Taylor length scale or Kolmogorov length scale) is an indication of turbulence enhancement or attenuation. The current study focused on the effects of sediment volume fraction on flow dynamics modulation with the same sediment diameter size, and such turbulent modulation criteria are not evaluated here.

V. CONCLUSIONS

The interactions between turbulent flow and the suspension of sediment were investigated using a mixing box and particle image velocimetry. Grid oscillation frequency, stroke length, mesh size, and total flow depth were held constant, while seven different loadings of quartz-density sediment 0.37–0.40 mm in diameter were tested (from 0% to 1.4% by volume). Two-dimensional PIV data were collected at 80 Hz at a single position, and fluid and sediment particles were discriminated using polarized filters placed onto the camera lens. From these images, spatially resolved mean flow, turbulent statistics, and particle concentration were calculated as a function of sediment loading.

The primary results from this experimental study are summarized below:

(1) In the clear-water condition, the maximum turbulent kinetic energy values were observed near the grid and they decreased toward the water surface. The mean kinetic energy was measurable and associated with secondary circulation cells within the box, turbulent length scales were similar to the grid mesh size and stroke lengths, and eddies were nearly spherical in shape.

(2) The presence of sediment in suspension decreased the mean kinetic energy, reducing the spatial extent of secondary circulation, and it altered the turbulent kinetic energy within the box. At relatively low sediment loadings, the turbulent kinetic energy increased near the grid and decreased away from the grid, but the total kinetic energy decreased.

(3) As sediment loading increased, total mean and turbulent kinetic energy, total suspended sediment, and fluid eddy viscosity all decreased, while the turbulent integral scales became larger and more anisotropic, resulting in progressively flatter eddies.

(4) Three characteristic length scales were recognized within the mixing box. These were related to the height of the secondary circulation cells D_s, the height of confined vertical mixing D, and the height of maximum suspended-sediment concentration D_c, and all of these decreased with increased sediment loading, suggesting a strong interaction between sediment resuspension and turbulence modulation.

(5) The nondimensional numbers controlling flow were the Rouse number R_o and the Richardson number R_i. As sand loading increased, R_o and R_i increased, and in all sediment-laden flow experiments, R_i was larger than R_o. Hence, sediment remained in suspension and formed a uniform high-concentration suspension layer with depth D_c, creating a stratified layer within the box. Dampening the secondary circulations and confining vertical turbulent mixing are both related to the vertical extent of the stratified layer, where turbulent integral length scales became anisotropic and altered the shape of the eddies. Above the stratified layer, turbulent length scales were almost isotropic and the eddies were more of a circular shape, similar to clear-water conditions. As sediment loading increased, both the total kinetic energy and the depth of the stratified layer decreased.

Mixing boxes with oscillating grids can be used to examine the turbulent transfer of flow and sediment dynamics similar to that observed in many geophysical flows [30]. The results presented here confirm that flow stratification effects due to the presence of suspended sediment greatly modulate time-averaged and turbulent flows, consistent with similar observation in rivers, estuaries, and near- and deep-marine environments.

ACKNOWLEDGMENTS

Fangyu Zeng is acknowledged for assisting with the preparation of the experimental setup and some of the data measurements. Two anonymous referees reviewed this paper and made many helpful suggestions on ways to improve it.

[1] J. Wainwright, A. J. Parsons, J. R. Cooper, P. Gao, J. A Gillies, L. Mao, J. D. Orford, and P. G. Knight, The concept of transport capacity in geomorphology, Rev. Geophys. **53**, 1155 (2015).

[2] J. Best, S. Bennett, J. Bridge, and M. Leeder, Turbulence modulation and particle velocities over flat sand beds at low transport rates, J. Hydraul. Eng. **123**, 1118 (1997).

[3] W. Hwang and J. K. Eaton, Homogeneous and isotropic turbulence modulation by small heavy (St ∼ 50) particles, J. Fluid Mech. **564**, 361 (2006).
[4] M. I. Cantero, S. Balachandar, A. Cantelli, and G. Parker, A simplified approach to address turbulence modulation in turbidity currents as a response to slope breaks and loss of lateral confinement, Environ. Fluid Mech. **14**, 371 (2014).
[5] V. A. Vanoni and G. N. Nomicos, Resistance properties of sediment-laden streams, J. Hydraul. Div. **85**, 77 (1959).
[6] N. L. Coleman, Effects of suspended sediment on the open-channel velocity distribution, Water Resour. Res. **22**, 1377 (1986).
[7] D. A. Lyn, Turbulence characteristics of sediment-laden flows in open channels, J. Hydraul. Eng. **118**, 971 (1992).
[8] J. Guo and P. Y. Julien, Turbulent velocity profiles in sediment-laden flows, J. Hydraul. Res. **39**, 11 (2001).
[9] O. Castro-Orgaz, J. V. Girldez, L. Mateos, and S. Dey, Is the von Kármán constant affected by sediment suspension? J. Geophys. Res.: Earth Surf. **117**, F04002 (2012).
[10] D. Zhong, L. Zhang, B. Wu, and Y. Wang, Velocity profile of turbulent sediment-laden flows in open-channels, Int. J. Sediment Res. **30**, 285 (2015).
[11] S. Kundu, M. Kumbhakar, and K. Ghoshal, Reinvestigation on mixing length in an open channel turbulent flow, Acta Geophys. **66**, 93 (2018).
[12] I. Nezu and R. Azuma, Turbulence characteristics and interaction between particles and fluid in particle-laden open channel flows, J. Hydraul. Eng. **130**, 988 (2004).
[13] M. Muste, K. Yu, I. Fujita, and R. Ettema, Two-phase versus mixed-flow perspective on suspended sediment transport in turbulent channel flows, Water Resour. Res. **41**, W10402 (2005).
[14] K. Noguchi and I. Nezu, Particle-turbulence interaction and local particle concentration in sediment-laden open-channel flows, J. Hydro-Environ. Res. **3**, 54 (2009).
[15] T. Revil-Baudard, J. Chauchat, D. Hurther, and P. A. Barraud, Investigation of sheet-flow processes based on novel acoustic high-resolution velocity and concentration measurements, J. Fluid Mech. **767**, 1 (2015).
[16] S. Balachandar and J. K. Eaton, Turbulent dispersed multiphase flow, Annu. Rev. Fluid Mech. **42**, 111 (2010).
[17] R. A. Gore and C. T. Crowe, Effect of particle size on modulating turbulent intensity, Int. J. Multiphase Flow **15**, 279 (1989).
[18] G. Hestroni, Particles-turbulence interactions, Int. J. Multiphase Flow **15**, 735 (1989).
[19] S. Elghobashi, On predicting particle-laden turbulent flows, Appl. Sci. Res. **52**, 309 (1994).
[20] F. Picano, W. P. Breugem, and L. Brandt, Turbulent channel flow of dense suspensions of neutrally buoyant spheres, J. Fluid Mech. **764**, 463 (2015).
[21] S. Wright and G. Parker, Density stratification effects in sand-bed rivers, J. Hydraul. Eng. **130**, 783 (2004).
[22] K. Ghoshal and B. S. Mazumder, Sediment-induced stratification in turbulent open-channel flow, Environmetrics **16**, 673 (2005).
[23] J. C. Winterwerp, Stratification effects by fine suspended sediment at low, medium, and very high concentrations, J. Geophys. Res. **111**, C05012 (2006).
[24] X. Yu, C. E. Ozdemir, T.-J. Hsu, and S. Balachandar, Numerical investigation of turbulence modulation by sediment-induced stratification and enhanced viscosity in oscillatory flows, J. Waterw. Port, Coastal, Ocean Eng. **140**, 160 (2014).
[25] Y. Noh and H. J. S. Fernando, Dispersion of suspended particles in turbulent flow, Phys. Fluids A **3**, 1730 (1991).
[26] C. E. Ozdemir, T. J. Hsu, and S. Balachandar, A numerical investigation of fine particle laden flow in an oscillatory channel: The role of particle-induced density stratification, J. Fluid Mech. **665**, 1 (2010).
[27] M. I. Cantero, M. Shringarpure, and S. Balachandar, Towards a universal criteria for turbulence suppression in dilute turbidity currents with non-cohesive sediments, Geophys. Res. Lett. **39**, L14603 (2012).
[28] B. Kneller, N.-A. Mohamad, S. Radhakrishnan, and E. Meiburg, Long-range sediment transport in the world's oceans by stably stratified turbidity currents, J. Geophys. Res.: Oceans **121**, 8608 (2016).

[29] A. Hooshmand, A. R. Horner-Devine, and M. P. Lamb, Structure of turbulence and sediment stratification in wave-supported mud layers, J. Geophys. Res.: Oceans **120**, 2430 (2015).
[30] H. E. Huppert, J. S. Turner, and M. A. Hallworth, Sedimentation and entrainment in dense layers of suspended particles stirred by an oscillating grid, J. Fluid Mech. **289**, 263 (1995).
[31] S. J. Bennett and J. L. Best, Particle size and velocity discrimination in a sediment-laden turbulent flow using phase Doppler anemometry, J. Fluids Eng. **117**, 505 (1995).
[32] S. J. Bennett, J. F. Atkinson, Y. Hou, and M. J. Fay, Turbulence modulation by suspended sediment in a zero mean-shear geophysical flow, in *Coherent Flow Structures at Earth's Surface*, edited by J. G. Venditti, J. L. Best, M. Church, and R. J. Hardy (Wiley, New York, 2013), p. 309.
[33] S. J. Bennett, Y. Hou, and J. F. Atkinson, Turbulence suppression by suspended sediment within a geophysical flow, Environ. Fluid Mech. **14**, 771 (2014).
[34] E. J. Hopfinger and J.-A. Toly, Spatially decaying turbulence and its relation to mixing across density interfaces, J. Fluid Mech. **78**, 155 (1976).
[35] I. P. D. De Silva and H. J. S. Fernando, Oscillating grids as a source of nearly isotropic turbulence, Phys. Fluids **6**, 2455 (1994).
[36] K. Dohan and B. R. Sutherland, Turbulence time scales in mixing box experiments, Exp. Fluids. **33**, 709 (2002).
[37] S. P. McKenna and W. R. McGillis, Observations of flow repeatability and secondary circulation in an oscillating grid-stirred tank, Phys. Fluids. **16**, 3499 (2004).
[38] S. M. Thompson and J. S. Turner, Mixing across an interface due to turbulence generated by an oscillating grid, J. Fluid Mech. **67**, 349 (1975).
[39] I. P. D. De Silva and H. J. S. Fernando, Experiments on collapsing turbulent regions in stratified fluids, J. Fluid Mech. **358**, 29 (1998).
[40] T. J. McDougall, Measurments of turbulence in a zero-mean-shear mixed layer, J. Fluid Mech. **94**, 409 (1979).
[41] S. B. Pope, *Turbulent Flow* (Cambridge University Press, Cambridge, 2000).
[42] H. Michallet and M. Mory, Modelling of sediment suspension in oscillating grid turbulence, Fluid Dyn. Res. **35**, 87 (2004).
[43] W. E. Dietrich, Settling velocity of natural particles, Water Resour. **18**, 1615 (1982).
[44] A. Aliseda, A. Cartellier, F. Hainaux, and J. C. Lasheras, Effect of preferential concentration on the settling velocity of heavy particles in homogeneous isotropic, J. Fluid Mech. **468**, 77 (2002).
[45] I. A. Hannoun, H. J. S. Fernando, and E. J. List, Turbulence structure near a sharp density interface, J. Fluid Mech. **189**, 189 (1988).
[46] N. Matsunaga, Y. Sugihara, T. Komatsu, and A. Masuda, Quantitative properties of oscillatig-grid turbulence in a homogeneous fluid, Fluid Dyn. Res. **25**, 147 (1999).
[47] J. C. Winterwerp, Stratification effects by cohesive and noncohesive sediment, J. Geophys. Res. **106**, 22559 (2001).
[48] M. R. Leeder, T. E. Gray, and J. Alexander, Sediment suspension dynamics and a new criterion for the maintenance of turbulent suspensions, Sedimentology **52**, 683 (2005).
[49] J. J. Orlins and J. S. Gulliver, Turbulence quantification and sediment resuspension in an oscillating grid chamber, Exp. Fluids. **34**, 662 (2003).